Quantifying Volumetric Differences in Infants with Hydrocephalus

by Alexis Bunnell

Hydrocephalus is the abnormal accumulation of cerebrospinal fluid which results in the dilation of the cerebral ventricles and is often associated with intraventricular pressure. Hydrocephalus occurs in ~1 in 1136 live births. Infants often present with symptoms such as irritability, lethargy, vomiting, a bulging of fontanelle, and above percentile head circumference. If left untreated, hydrocephalus can potentially lead to death. Currently, pediatric hydrocephalus diagnosis is more dependent on interpretation of anatomical changes rather than clinical exams. Three pediatric patients with enlarged ventricles were recruited from M Health and underwent structural MRIs. An additional participant with an enlarged ventricle was identified from an incidental finding in the Baby Connectome Project (BCP). For these four cases, MRI scans from age-matched healthy controls were also pulled from the BCP. An open-source deep-learning model (BIBSNet) was utilized to create full brain segmentations. These segmentations were manually corrected with ITK-SNAP for the participants with enlarged ventricles, as current segmentation models do not perform well on patients with enlarged ventricles. Then volumetric data for cortical and select subcortical structures and regions (lateral ventricle, inferior lateral ventricle, cerebral white matter, cerebral cortex, thalamus, caudate nucleus, hippocampus, amygdala) were pulled and compared between clinical patients and age-matched healthy controls. Comparisons found that there are differences in cortical and subcortical volume metrics between typically developing infants and the clinical participants based on severity of diagnosis with incidental unilateral ventriculomegaly, ventriculomegaly, moderate hydrocephalus, or severe hydrocephalus above and beyond the expected differences in ventricle volume. By further quantifying and understanding differences between these clinical infants and the healthy control infants, we can work to better understand the full effects of hydrocephalus on brain development which can be influential in research and eventually clinical settings.

Introduction

Hydrocephalus occurs in ~1 in 1136 live births (Isaacs et al., 2018). Hydrocephalus is defined as the abnormal accumulation of cerebrospinal fluid which results in the dilation of the cerebral ventricles and is often associated with intraventricular pressure (Wright et al., 2016). Hydrocephalus diagnosis is found more often in premature infants than full term infants of ~40 weeks of pregnancy (Koleva & De Jesus, 2023). In-patient care of pediatric hydrocephalus in the United States costs approximately $2 billion a year, with additional costs for outpatient care (Isaacs et al., 2018). There are substantial negative outcomes associated with hydrocephalus including developmental delays, psychomotor delays, gait difficulties, and death (Isaacs et al., 2018). The prevalence and severity of these symptoms are dependent on the etiology.

Hydrocephalus etiologies share features of enlarged ventricles and CSF accumulation but are distinguished by the cause of CSF accumulation. The two broad categories of hydrocephalus include communicating and noncommunicating based on the location and/or presence of an obstruction. Communicating hydrocephalus is characterized by an excess of CSF as a result of poor CSF absorption. There is no fluid blockage in the ventricular system into the subarachnoid space (Wright et al., 2016). Noncommunicating (obstructive) hydrocephalus is characterized by an excess of CSF as a result of a blockage in the ventricular system reducing flow into the subarachnoid space (Wright et al., 2016). Noncommunicating hydrocephalus is often the result of congenital or acquired factors that obstruct normal CSF absorption (Cheng et al., 2015). Noncommunicating hydrocephalus can be further classified based on the locations and causes of obstruction. Obstruction can occur at the levels of the foramen of Monro, the aqueduct, or the foramina

of Luschka and Magendie (Maller & Gray, 2016). In an investigation of 236 infants with developmental hydrocephalus that worked to classify their diagnosis into five clinical-radiographic categories, 59 infants with the aqueductal obstruction were identified. Hydrocephalus associated with aqueductal obstruction had the earliest onset and was associated with the highest ventricular dilation severity as well as the worst developmental outcomes, including need for physical and speech therapy, as well as epilepsy presence (Tully et al., 2016).

Diagnosis

Hydrocephalus diagnosis is based on clinical symptoms, imaging, and CSF pressure readings and can be influenced by the patient's age, speed of onset, hydrocephalus etiology, and, if applicable, location of obstruction (Koleva & De Jesus, 2023). This makes early intervention difficult because pediatric patients aren't able to fully and verbally participate in clinical exams. As a result, intervention often occurs only once head circumference is very large (Peña Pino et al., 2024). Specifically, the neurological aspect of the exam involves tests of muscle strength and reflexes; coordination and balance; vision, eye moment, and hearing; and mental functioning and mood which is harder to recognize in infants (NINDS, 2025).

Young infants often present with symptoms such as irritability, lethargy, vomiting, a bulging fontanelle (an infant's soft spot), and above percentile head circumference. (Kestle, 2003). Current pediatric hydrocephalus treatment is reliant on the interpretation of anatomical differences, such as the size and shape of the ventricles, especially the third ventricle, transependymal flow, subarachnoid space shape, and CSF flow (Peña Pino et al., 2024). Anatomical differences, which are visualized by MRI along with an understanding of the patient from the clinical examination, are key to proper and early hydrocephalus diagnosis (Kestle, 2003).

Ventriculomegaly is the dilation of ventricles and differs from hydrocephalus, which is a brain condition that includes ventriculomegaly as a result of intracranial pressure (Patel et. al., 2020). The primary way to distinguish between hydrocephalus and ventricular enlargement is the enlargement of the third ventricle in its inferior and anterior, dilation of the temporal horns of the lateral ventricles, and a less clear ventricular border as a result of transependymal flow in hydrocephalus patients (Wright et al., 2016).

Cerebrospinal Fluid

The accumulation of cerebrospinal fluid (CSF) for patients with hydrocephalus can be a result of obstruction to the natural flow of CSF, impaired CSF absorption into the venous system, or excess CSF production (Koleva & De Jesus, 2023). Transependymal flow is the movement of CSF across the ependymal lining of the ventricles and into the brain. The choroid plexus is a capillary network lined by specialized ependymal cells (Javed et al., 2023). Choroid plexus attached to the lining of the ventricles is responsible for CSF production with the majority of CSF production being in the lateral ventricles specifically (Wright et al., 2016). Additionally, the choroid plexus is responsible for the blood-CSF barrier. From the choroid plexus in the lateral ventricles, CSF flows through the foramen of Monro into the third ventricle. The CSF then flows through the cerebral aqueduct into the fourth ventricle. Finally, the CSF exits from the fourth ventricle into the subarachnoid space through the foramina of Luschka and Magendie (Maller & Gray, 2016). From the subarachnoid space in the brain and spinal cord, the CSF is then reabsorbed through the cerebral venous system (Haines & Mihailoff, 2017). Another hallmark feature of pediatric hydrocephalus transependymal flow is the enlargement of the anterior and inferior parts of the third ventricle, lateral ventricles temporal horns dilation, and an unclear ventricular border as a result of CSF going across the ventricle ependymal walls (Wright et al., 2016).

Treatments

For hydrocephalus treatment, shunts are used to divert CSF from the ventricular system to the subarachnoid space. This is achieved using a small silicone tube to carry the CSF to a different body cavity for reabsorption. These shunts are seen as successful when the ventricle size decreases, which can be visualized with structural anatomy from an MRI. Endoscopic Third Ventriculostomy (ETV) is another option used to help treat patients diagnosed with

obstructive or noncommunicating hydrocephalus. This procedure is helpful in hydrocephalus caused by a blockage of the flow of CSF. ETV works by making a bypass through the thin membrane in the floor of the third ventricle because the most common site of blockage is the small pathway between the third and fourth ventricle of the brain, known as the foramen of Monro. ETV treatment failure is much higher in the younger patients, especially those under 6 months (Kulkarni et al., 2016). This is most likely because the patient does not have a purely obstructive cause of hydrocephalus, which is difficult to diagnose in infant populations (Beni-Adani et al., 2006).

The type of treatment a pediatric patient has is dependent on the type and severity of hydrocephalus, which for infants is primarily diagnosed based on structural MRI imaging. Not all infants with hydrocephalus require the placement of a shunt, and the decision encompasses factors such as the fragility and infection risk of the patient (Peña Pino et al., 2024). Pediatric patients with communicating hydrocephalus presenting with CSF accumulation due to poor CSF absorption utilize an extracranial shunt for treatment. Additionally, pediatric patients with communicating hydrocephalus presenting with atypical obstructions and absorption are treated with a shunt (Beni-Adani et al., 2006). Pediatric patients with hydrocephalus presenting with a primarily obstructive cause and minor absorptive cause or with a purely obstructive cause would typically be treated with ETV followed by a temporary CSF drainage (Beni-Adani et al., 2006).

Typical Brain Development

By 6 years old, the total brain volume is approximately 90% of the adult brain volume (Lebel & Deoni, 2018). For typically developing infants, from birth there are large increases in overall gray matter volumes across the first year of life which is then followed by a significant but smaller increase in the second year of life (Gilmore et al., 2012). Myelination occurs rapidly over the first 5 years of life through the caudal-cranial, posterior to anterior arc, which overall improves brain connectivity (Lebel & Deoni, 2018). Therefore, it is important when making comparisons between clinical participants to separate based on age and adjust to correct ages to account for prematurity.

Current Gaps in Knowledge

Hydrocephalus classification in pediatrics is different from adult patient populations because the sources of hydrocephalus, diagnosis protocols, and treatment choices are more complex (Beni-Adani et al., 2006). Currently, anatomical and clinical references for information regarding pediatric hydrocephalus is limited to severe cases of hydrocephalus (Tully et al., 2016). This makes it difficult to have earlier clinical decision making because of the lack of more differentiated imaging biomarkers to inform hydrocephalus diagnosis in severity and etiology (Peña Pino et al., 2024). Additionally, because pediatric hydrocephalus diagnosis is currently more dependent on interpretation of anatomical difference rather than clinical exams, there is a need to look for other ways to quantify early disease detection. Through this study, we want to quantify volumetric differences in infants with hydrocephalus by investigating differences in cortical and subcortical volume metrics in infants with hydrocephalus compared to typically developing infants. This topic has not been explored in depth before, and this study could serve as a stepping point for a full quantification in the future. First, we expect there to be differences in cortical and subcortical volume metrics between typically developing infants and hydrocephalus infants. Secondly, we expect that volumes of the lateral ventricles and inferior lateral ventricles of clinical participants will be larger than the age-matched healthy controls, because ventricle dilation is a common symptom of hydrocephalus (Patel et. al., 2020). Thirdly, because of the large ventricles typically associated with hydrocephalus diagnosis, we expect that the volumes of the cerebral white matter and cerebral cortex of clinical participants will be smaller than the age-matched healthy controls based on past MRI imaging of hydrocephalus (Koleva & De Jesus, 2023). Lastly, we expect that the volumes of subcortical structures/regions such as the thalamuses, caudate nucleuses, hippocampus, and amygdalae of clinical participants will also be smaller than the age-matched healthy controls, because based on the past MRI imaging of hydrocephalus, the large ventricles appear to overtake these structures (Koleva & De Jesus, 2023). The more information that we have about the

anatomical differences between these clinical infants and typical infants the more knowledge we will have of brain metrics for pediatric hydrocephalus patients to better diagnose and select treatments in the future.

Materials and Methods

Participants

The study included 154 participants, 4 of which were clinical participants and the remaining were age-matched healthy controls (0 to 16.7 months old). Typically developing infants from the Baby Connectome Project (BCP) were selected as the healthy controls. The clinical participants were classified based on severity of diagnosis with incidental unilateral ventriculomegaly, ventriculomegaly, moderate hydrocephalus, and severe hydrocephalus respectively (Figure 1). The clinical participant cohort only included infant participants available during the study period that met the inclusion criteria of ventriculomegaly or hydrocephalus. Demographic characteristics were not assessed in the present study because the primary goal was to assess volume differences associated with hydrocephalus severity. Due to prematurity of birth for the clinical participants, corrected ages were determined to allow for more accurate comparisons of structural volume (Table 1). Corrected age was calculated by subtracting the age at scan (months) by the months born premature. The corrected age adjusted the age of most of the clinical participants to account for their premature birth.

Clinical participants were identified at clinical diagnosis of prematurity once a head ultrasound demonstrated intraventricular hemorrhage and or at any time during the first 6 months of life with a clinical diagnosis of hydrocephalus. Clinical participants were recruited based on this clinical diagnosis from M Health Fairview Pediatric Clinic. Parents of all participants provided permission and informed consent prior to participation. The University of North Carolina at Chapel Hill (UNC) and the University of Minnesota (UMN) Institutional Review Boards approved all procedures. Age-matched healthy control participants from BCP were recruited based on state-wide birth records from existing registries at UNC and UMN (Howell et al., 2019). Additionally, participants were recruited from community resources and related hospital systems. To recruit the youngest infants, some expectant or new mothers at "The Birthplace" at UMN and the UNC Hospitals Newborn Nursery were approached to participate in the study.

Materials

High resolution structural MRIs were conducted for the pediatric typically developing infants (Howell et al., 2019). Magnetic resonance imaging (MRI) does not emit ionizing radiation but utilizes radio waves and magnets to create detailed imaging of internal structures in the body (Wright et al., 2016). Fast-sequenced MRI is a noninvasive technique that can be used for non-anesthetized sleeping infants (Lebel & Deoni, 2018). MRI, because of the anatomical detail, can highlight the presence of transependymal flow, tumors, or another pathology that might be causing hydrocephalus (Wright et al., 2016). MRI doesn't have ionizing radiation exposure but is often longer than other neuroimaging techniques such as CT (Wright et al., 2016). T1 and T2-weighted MRI scans are typically used to measure volume, cortical thickness, and surface area of brain structures (Lebel & Deoni, 2018). Fast-sequenced MRIs were utilized for all participants and allowed for high quality data. The Baby and Infant Brain Segmentation Neural Network (BIBSNet) is an open-source community model that utilizes data augmentation and a large sample size of manually segmented images to create general brain segmentations for individual participants (Hendrickson et al., 2023). It creates a model that is matched to a specific infant MRI based on neuronal developmental status, age, quality and data acquisition (Hendrickson et al., 2023). Neuronal developmental status is the process of neuronal networks forming in the infant into adulthood. BIBSNet was built based on previous deep learning infant segmentations (nnU-Net) but does not require the removal of skull, brainstem, or cerebellum from the images, which improves its preprocessing speed before inferences (Hendrickson et al., 2023). T1-weighted imaging reflects longitudinal relaxation time where T2-weighted images reflect transverse relaxation time. Visual differences in these images reflect differences in myelination and water content (Lebel & Deoni, 2018). ITK-SNAP is a software

tool with a graphical interface that can be utilized to manually correct segmentations of the T1 and T2 MRI images (Yushkevich et al., 2019). R-studio was utilized to compare and analyze differences or similarities across the quantitative data.

Procedure

High resolution structural MRIs were conducted on a 3T Siemens Prisma MRI Scanner at the University of Minnesota for all the participants. BIBSNet was used to create general brain segmentations. T1 and T2 images were registered with BIBSnet in overlaid space as part of the BCP (Baby Connectome Project) processing pipeline. When the T1 and T2 images did not coregister well, we selected the best image between the T1 and T2 images. Because BIBSnet was developed for typical developing infants, it did not perform well for infants with hydrocephalus (Figure 2). ITK-SNAP was utilized to manually correct segmentations of the T1 and T2 MRI images as needed for the clinical participants. Corrected segmentations could then be returned to the native space by conducting the inverse of the transformation by BIBSnet. This was an individual analysis of each clinical participant to a group of age-matched healthy controls. Cortical and subcortical structures/regions of interest (lateral ventricle, inferior lateral ventricle, cerebral white matter, cerebral cortex, thalamus, caudate nucleus, hippocampus, amygdala) were selected to best quantify the differences between clinical participants and their age-matched healthy controls. These are visualized in Figure 3, and some of their presumed functions are summarized in Table 2. Volumes were estimated for all participants for cortical and subcortical structures/regions of interest and then compared between clinical participants and their age-matched healthy controls by hemisphere and structure/region. R-studio was utilized to create boxplots for these comparisons. Additionally, Z scores were calculated for each of the clinical participants using the mean and standard deviations of the age-matched cohort data to quantify the differences between clinical participants and healthy controls. Z-scores were calculated for each cortical and subcortical volume metrics for each clinical participant by their age group cohort (Equation 1). Z-scores determined how far the clinical participant data point was from the mean of the entire age-matched cohort in terms of standard deviations from the mean.

Results

Boxplots of volumetric voxels of cortical and subcortical structures/regions of interest by hemisphere are used to visualize comparisons between the clinical participants and age-matched healthy controls (Figure 4). Age-matched cohort is used to refer to the cohort of participants including the clinical participant and the age-matched healthy controls. They are labeled based on the severity of the clinical diagnosis of the clinical participant. Each boxplot is arranged from left to right by age-matched cohorts depending on severity of the diagnosis of the clinical participant within that cohort. Clinical participants are highlighted in color based on diagnosis to clearly see how the participant compares to the distribution of age-matched healthy controls. Outliers are values that lie 1.5 times outside the interquartile range (IQR), above the third quartile (Q3) or below the first quartile (Q1) of the boxplot. Outliers are represented within the boxplots as individual black points plotted beyond the whiskers and represent large deviations from the overall distribution of the data. Z scores for each of the clinical participants using the mean and standard deviations of the data were used to quantify the differences between clinical participants and healthy controls (Table 3). Z-scores determined how far the clinical participant data point was from the mean of the entire age-matched cohort in terms of standard deviations from the mean. A positive z score indicates that the data point was above the mean, whereas a negative z score indicates that it was below the mean. Additionally, z-score between -2 or +2 of the mean were considered within the normal range of the age-matched cohort.

Based on the boxplots for the clinical participant with incidental unilateral ventriculomegaly, the volumes for the right lateral ventricle and inferior lateral ventricle are considered outliers. The volumes bilaterally for the cerebral white matter, cerebral cortex, amygdala, and right hippocampus are beyond the IQR. The volumes bilaterally for thalamus, caudate, left lateral ventricle and inferior lateral

ventricle, and left hippocampus are within the IQR. Based on the boxplots for the clinical participant with ventriculomegaly, the volumes bilaterally for the lateral ventricles, inferior lateral ventricles, caudate, hippocampus, are considered outliers. The volumes bilaterally for the cerebral white matter, left hippocampus, and left amygdala are beyond the IQR. The volumes bilaterally for the cerebral cortex, thalamus and right amygdala are within the IQR. Based on the boxplots for the clinical participant with moderate hydrocephalus, the volume bilaterally for the lateral ventricles, inferior lateral ventricles, cerebral cortex, thalamus, caudate, hippocampus, and left amygdala are considered outliers. The volume of the right amygdala is beyond the IQR, whereas the volume bilaterally for the cerebral white matter is within the IQR. Based on the boxplots for the clinical participant with severe hydrocephalus, the volume bilaterally for the lateral ventricles, inferior lateral ventricles, thalamus, caudate, and hippocampus are considered outliers, whereas the volume bilaterally for the cerebral white matter, cerebral cortex, and amygdala is within the IQR.

The clinical participant with incidental unilateral ventriculomegaly had z-scores above normal range for the lateral ventricle, inferior lateral ventricle, and cerebral cortex on only the right hemisphere of the brain. The clinical participant with ventriculomegaly had z-scores above normal range bilaterally for lateral ventricle and inferior lateral ventricle. The clinical participant with ventriculomegaly had z-scores below normal range bilaterally for caudate and hippocampus. Additionally, the clinical participant with ventriculomegaly had z-scores within normal range bilaterally for cerebral white matter, cerebral cortex, thalamus, and amygdala. The clinical participant with moderate hydrocephalus had z-scores above normal range bilaterally for lateral ventricle and inferior lateral ventricle. The clinical participant with moderate hydrocephalus had z-scores below normal range bilaterally for cerebral cortex, thalamus, caudate, hippocampus, and amygdala. Additionally, the clinical participant with moderate hydrocephalus had z-scores within normal range bilaterally for cerebral white matter. The clinical participant with severe hydrocephalus had z-scores above normal range bilaterally for lateral ventricle and inferior lateral ventricle. The clinical participant with severe hydrocephalus had z-scores below normal range bilaterally for thalamus, caudate, and hippocampus. Additionally, the clinical participant with severe hydrocephalus had z-scores within normal range bilaterally for cerebral white matter and cerebral cortex.

Tables and Figures

Clinical Participant Diagnosis	Gestational Age	Age at Scan (months)	Corrected Age (months)	Age Matched BCP Healthy Control Ranges (months)
Incidental Unilateral Ventriculomegaly	~40 weeks (Full-term)	16	NA	15.25-16.75
Ventriculomegaly	~27 weeks	9.8	6.8	7.55-6.05
Moderate Hydrocephalus	~23 weeks	12.2	8.3	7.55-9.05
Severe Hydrocephalus	~25 weeks	4.5	1.1	0.35-1.85

Table 1. Clinical participant information. Corrected age is adjusting the age to account for preterm birth.

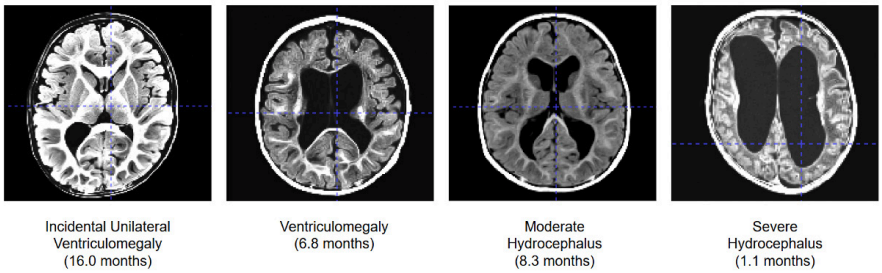

Figure 1. Structural T1 MRIs of the clinical participants to visualize anatomical differences in order of severity (right to left).

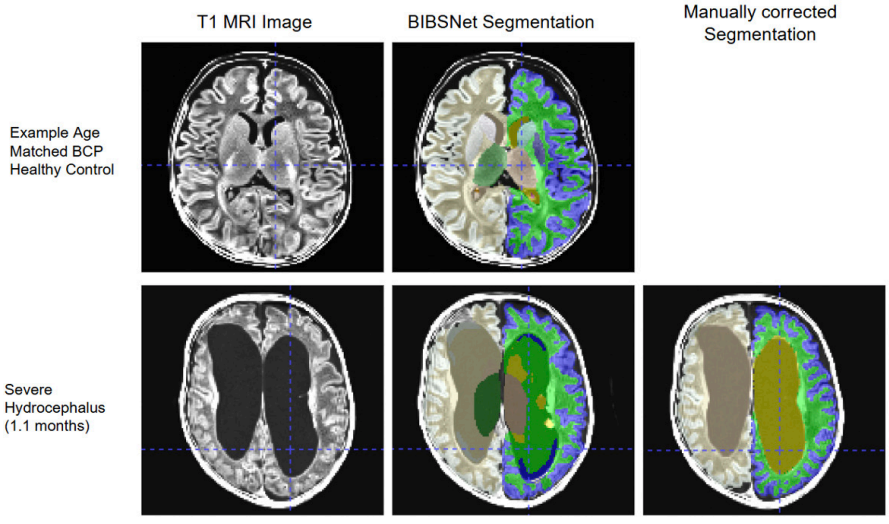

Figure 2. Axial view of T1 MRI image and corresponding segmentations of the clinical participant with Severe Hydrocephalus (1.1 months) compared with an example of an age-matched BCP healthy control.

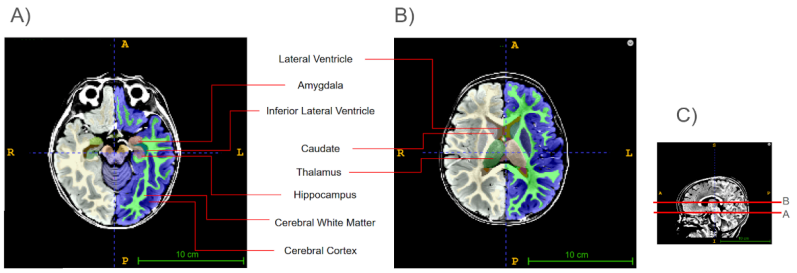

Figure 3. (A) and (B) Axial view of T1 weighted images of a BCP healthy control (8.3 months) with cortical and subcortical labels. (C) Sagittal view with locations of corresponding slices.

Structure	Function
Lateral Ventricle	Subcortical area responsible for production and circulation of cerebrospinal fluid (CSF)
Inferior Lateral Ventricle	Inferior subdivision of lateral ventricle subcortical area that helps to facilitate the circulation of CSF
Cerebral White Matter	Cortical region that utilizes fiber pathways of axons linking cerebral cortical areas and subcortical structures to facilitate neural circuits for sensorimotor function, intellect, and emotion
Cerebral Cortex	Cortical region that aids in perception and higher motor function with sensory information processing and motor functions integration
Thalamus	Subcortical structure that processes sensory information going to the cerebral cortex and motor information going to the brainstem and spinal cord
Caudate Nucleus	Subcortical structure that plays a role in planning the execution of movement, learning, memory, reward, motivation, and emotion
Hippocampus	Subcortical structure that is primarily involved with memory formation, spatial navigation,and memory consolidation
Amygdala	Subcortical structure that processes the emotional information gathered from the autonomic system and the hypothalamus and is involved in hormone secretion

Table 2. Functions of cortical and subcortical structures/regions of interest (Ludwig, 2025)

$$z = \frac{x - \mu}{\sigma}$$

Equation 1. z is the z-score. χ is the individual clinical participant's volume point for selected cortical and subcortical structures/regions of interest, μ is the mean volume of the age-matched cohort for the same selected cortical and subcortical structures/regions of interest, and σ is the standard deviation of that cohort. Z-scores were used to standardize values and assess whether clinical participant data points deviated substantially from normative expectations of volume for the age-matched cohort.

Comparisons of Cortical and Subcortical Volume Metrics of Clinical Patients by Age Group

Clinical Participant Information		*Diagnosis*	*Incidental Unilateral Ventriculomegaly*	*Ventriculomegaly*	*Moderate Hydrocephalus*	*Severe Hydrocephalus*
		Age (Months)	16.0	6.8	8.3	1.1
			Z-scores			
Cortical and Subcortical Structures/Regions by Hemisphere	Left	**Cerebral White Matte**	1.322	1.246	-0.809	-0.134
		Cerebral Cortex	1.725	-0.373	-3.253	-0.219
		Lateral Ventricle	0.314	5.929	5.339	4.683
		Inferior Lateral Ventri	1.727	4.816	4.703	4.688
		Thalamus	0.650	0.552	-4.871	-2.513
		Caudate	-0.488	-2.850	-5.195	-3.405
		Hippocampus	0.737	-2.116	-3.794	-3.282
		Amygdala	1.597	-1.514	-3.439	1.237
	Right	**Cerebral White Matte**	1.161	0.935	-0.572	-0.373
		Cerebral Cortex	2.133	-0.412	-2.898	-0.311
		Lateral Ventricle	5.974	6.231	5.373	4.686
		Inferior Lateral Ventri	6.651	5.697	4.128	4.689
		Thalamus	0.731	-0.634	-4.024	-3.068
		Caudate	-0.260	-4.057	-5.259	-3.137
		Hippocampus	1.197	-3.076	-3.899	-3.172
		Amygdala	1.676	-0.466	-2.404	0.553

Table 3. Comparisons of Cortical and Subcortical Volume Metrics of Clinical Patients by Age Group. Data values highlighted in color are considered beyond the normal range of -2 standard deviations (blue) or +2 standard deviations (purple) from the mean. Ages are adjusted for prematurity.

A)

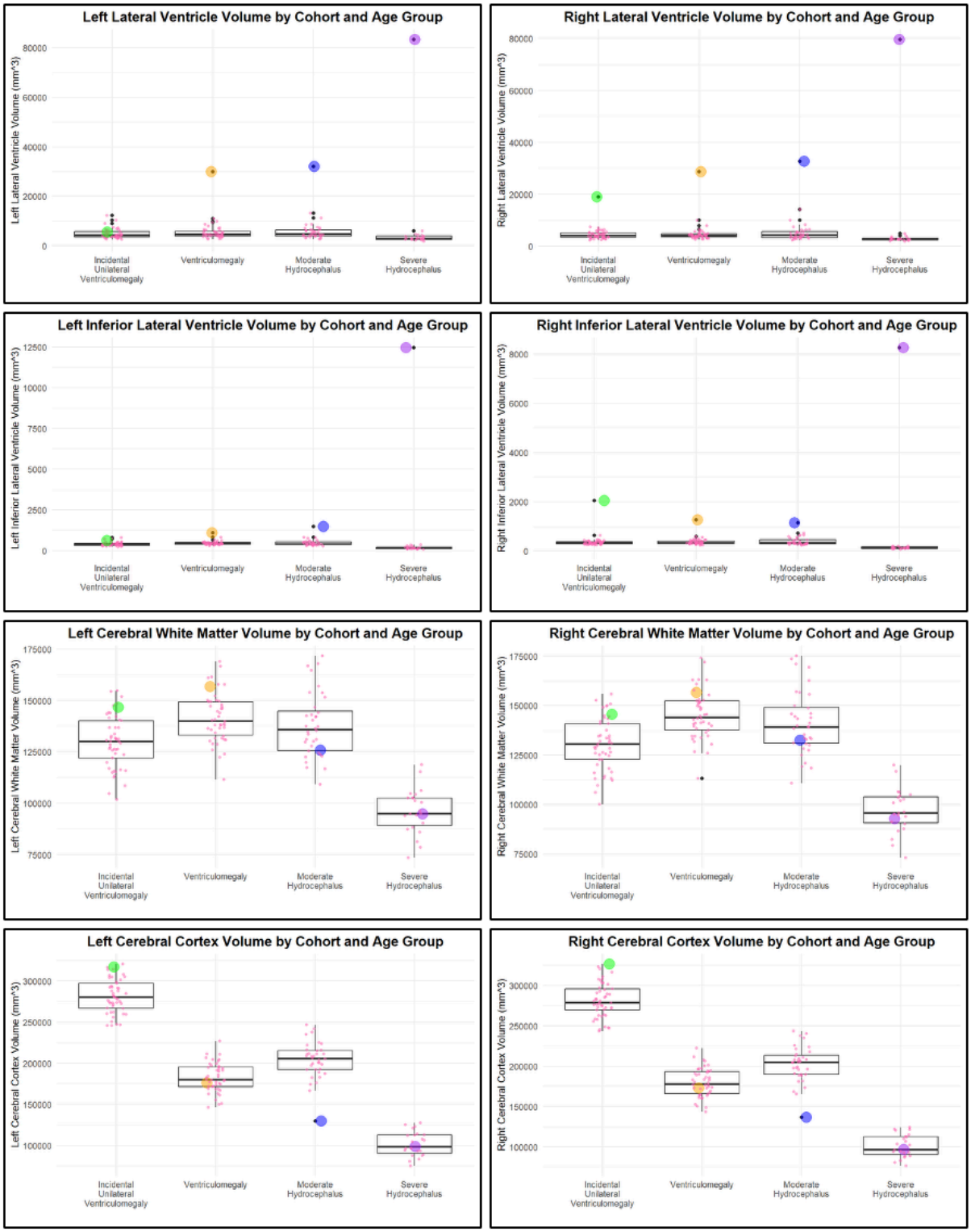
Left Lateral Ventricle Volume by Cohort and Age Group
Left Lateral Ventricle Volume (mm^3)
Right Lateral Ventricle Volume by Cohort and Age Group
Right Lateral Ventricle Volume (mm^3)
Left Inferior Lateral Ventricle Volume by Cohort and Age Group
Left Inferior Lateral Ventricle Volume (mm^3)
Right Inferior Lateral Ventricle Volume by Cohort and Age Group
Right Inferior Lateral Ventricle Volume (mm^3)
Left Cerebral White Matter Volume by Cohort and Age Group
Left Cerebral White Matter Volume (mm^3)
Right Cerebral White Matter Volume by Cohort and Age Group
Right Cerebral White Matter Volume (mm^3)
Left Cerebral Cortex Volume by Cohort and Age Group
Left Cerebral Cortex Volume (mm^3)
Right Cerebral Cortex Volume by Cohort and Age Group
Right Cerebral Cortex Volume (mm^3)
Incidental Unilateral Ventriculomegaly
Ventriculomegaly
Moderate Hydrocephalus
Severe Hydrocephalus

B)

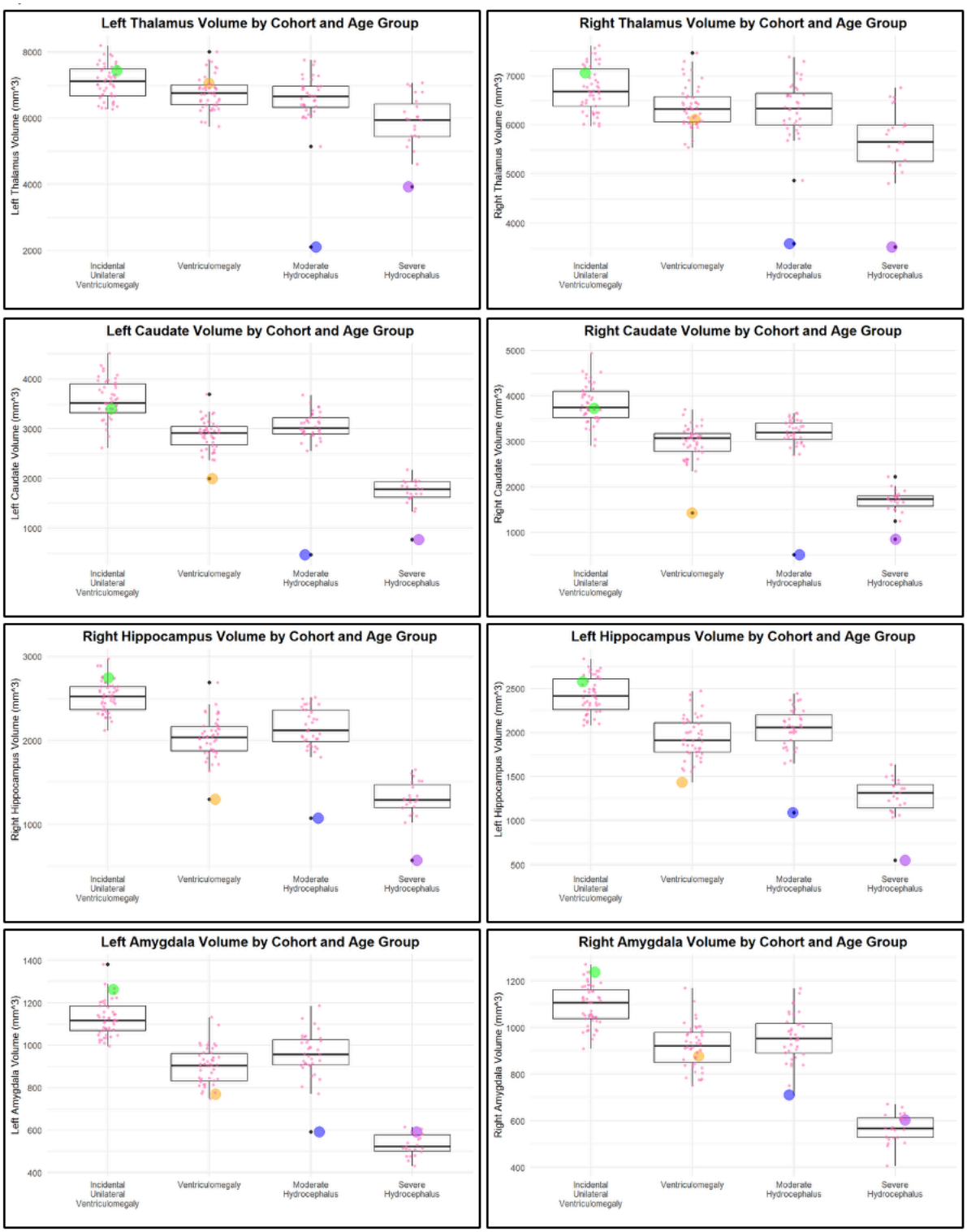

Figure 4. Comparison of volumes of cortical (A) and subcortical (B) structures/regions of interest of clinical participants to age matched healthy controls by hemisphere and structure/region.

Discussion

There are differences in cortical and subcortical volume metrics between typically developing infants and infants with hydrocephalus. As expected, there were differences in volume of lateral ventricles and inferior lateral ventricles between the clinical patients and the age-matched healthy controls. The level of impact appeared to track with the severity of diagnosis with clinical participants with a hydrocephalus diagnosis having volumes of thalamus, caudate, and hippocampus that were much smaller compared to the age-matched healthy controls. The thalamus is related to sensory processing (Ludwig, 2025), and therefore, a smaller thalamus could have an impact on related sensory networks. Similarly, the caudate is related to planning the execution of movement, learning, memory, reward, motivation, and emotion (Ludwig, 2025), which suggests that smaller volume of caudate could have implications in neurodevelopment and decision making. Additionally, the hippocampus is involved in memory formation, spatial navigation, and memory consolidation (Ludwig, 2025), which suggest that reductions in hippocampal volume could affect cognitive development and processing. It was surprising to note that the cerebral white matter and cerebral cortex appeared to be less impacted. Clinician collaborators on the project noted that this might be because of the head circumference expanding, compensating for the increased ventricles. For both the moderate and severe hydrocephalus participants, bilaterally the volumes for the cerebral cortex were within the IQR of age-matched healthy controls.

This pattern appears to track with the location of the thalami, caudate, and hippocampi being adjacent to the lateral and inferior lateral ventricles, which are impacted in the clinical cases. It is interesting to note that these structures were impacted and not the amygdala or cortical gray matter. This would make sense because the amygdala, cerebral white matter, and cerebral cortex are not as central as the thalami, caudate, and hippocampi, which would protect them from volume loss due to ventricle dilation or intraventricular pressure. The minimal impact on the amygdala, cerebral white matter, and cerebral cortex may indicate that structures closer to the enlarged ventricles, such as the thalami, caudate, and hippocampi, are more at risk to reduced volume because of hydrocephalus.

This quantification of some specific structures impacted (thalamus, caudate, and hippocampus) in participants with hydrocephalus gives insight as to which structures may be important markers for earlier hydrocephalus detection based on structural MRIs. The bilateral thalamus, caudate, and hippocampus could be used to improve how we detect and assess the severity of hydrocephalus. We can use this knowledge of specific brain metrics patterns for pediatric hydrocephalus patients to guide further exploration in studies regarding earlier hydrocephalus detection. Additionally, the structural volume abnormalities detected in these regions could help explain some of the negative outcomes associated with hydrocephalus, including developmental delays, psychomotor delays, gait difficulties, and death (Isaacs et al., 2018) observed in pediatric hydrocephalus populations.

There are limitations to this case study due to the small sample size, making it difficult to make exact inferences about patterns, especially considering each participant was at a different age. Based on this study, the patterns for volumetric differences between clinical participants and age-matched healthy controls clearly indicate the need for future exploration and research into these topics. If we had more subjects, we could attempt to separate and compare data based on severity or age to have a more generalized understanding of volumetric differences based on those parameters specifically.

A current treatment of hydrocephalus is a shunt insertion, which serves to divert CSF from the ventricular system to a different body cavity (Kestle, 2003). Future directions include looking at these data longitudinally and considering the data from a pre- and post-shunt insertion perspective. We would expect that the volumetric differences between clinical participants post-shunt insertion would show volumes closer to age-matched healthy controls, based on previous studies showing significant improvement towards healthy control values post-operatively in terms of reversibility of white matter changes (Peña Pino et al., 2024). Additionally, it would be interesting to have more participants to fully conceptualize the patterns in the volumetric differences across more cortical structures over different ages. It would also be interesting to pull cognitive and behavioral study data and make comparisons to the volumetric

data. These comparisons would be useful because the relationships could give insight into the effect of hydrocephalus on an infant's cognition and behavior. Future studies could investigate if the volumes of thalami, caudate, and hippocampi are associated with functional deficits associated with these regions. Understanding the full effects of hydrocephalus on brain development is crucial to improving diagnostics and treatments for pediatric hydrocephalus.

Acknowledgements

I would like to thank Dr. Jed Elison for his mentorship and guidance throughout this honors thesis. I am grateful to members of his lab for their support and assistance throughout this project. I would especially like to thank Dr. Sally Stoyell and Kimberly Weldon for their help with data collection, analysis, and project development. I also thank Dr. Isabela Peña Pino, Dr. Carolina Sandoval-Garcia, Jesse Kowalski, Jacob Lundquist, and Julia Moser for their feedback and support. I am very grateful for the support of Dr. Kathleen Thomas and Dr. Anna Mosser, who served on my thesis committee and offered thoughtful feedback on this work. Finally, I would like to acknowledge the University of Minnesota–Twin Cities College of Biological Sciences and University Honors Program for their support throughout my undergraduate studies.

References

Beni-Adani, L., Biani, N., Ben-Sirah, L., & Constantini, S. (2006). The occurrence of obstructive vs absorptive hydrocephalus in newborns and infants: Relevance to treatment choices. *Child's Nervous System, 22*(12), 1543–1563. https://doi.org/10.1007/s00381-006-0193-5

Gilmore, J. H., Shi, F., Woolson, S. L., Knickmeyer, R. C., Short, S. J., Lin, W., Zhu, H., Hamer, R. M., Styner, M., & Shen, D. (2012). Longitudinal development of cortical and subcortical gray matter from birth to 2 years. *Cerebral Cortex, 22*(11), 2478–2485. https://doi.org/10.1093/cercor/bhr327

Haines, D. E., & Mihailoff, G. A. (2017). The ventricles, choroid plexus, and cerebrospinal fluid. In *Fundamental neuroscience for basic and clinical applications* (5th ed., p. 516). Elsevier.

Hendrickson, T. J., Reiners, P., Moore, L. A., Lundquist, J. T., Fayzullobekova, B., Perrone, A. J., Lee, E. G., Moser, J., Day, T. K. M., Alexopoulos, D., Styner, M., Kardan, O., Chamberlain, T. A., Mummaneni, A., Caldas, H. A., Bower, B., Stoyell, S., Martin, T., Sung, S., ... Feczko, E. (2023). BIBSNet: A deep learning baby image brain segmentation network for MRI scans. *Neuroscience.* https://doi.org/10.1101/2023.03.22.533696

Howell, B. R., Styner, M. A., Gao, W., Yap, P.-T., Wang, L., Baluyot, K., Yacoub, E., Chen, G., Potts, T., Salzwedel, A., Li, G., Gilmore, J. H., Piven, J., Smith, J. K., Shen, D., Ugurbil, K., Zhu, H., Lin, W., & Elison, J. T. (2019). The UNC/UMN Baby Connectome Project (BCP): An overview of the study design and protocol development. *NeuroImage, 185,* 891–905. https://doi.org/10.1016/j.neuroimage.2018.03.049

Isaacs, A. M., Riva-Cambrin, J., Yavin, D., Hockley, A., Pringsheim, T. M., Jette, N., Lethebe, B. C., Lowerison, M., Dronyk, J., & Hamilton, M. G. (2018). Age-specific global epidemiology of hydrocephalus: Systematic review, metanalysis and global birth surveillance. *PLOS ONE, 13*(10), e0204926. https://doi.org/10.1371/journal.pone.0204926

Javed, K., Reddy, V., & Lui, F. (2023). Neuroanatomy, choroid plexus. In StatPearls [Internet]. StatPearls Publishing. https://www.ncbi.nlm.nih.gov/books/NBK538156/

Kestle, J. R. W. (2003). Pediatric hydrocephalus: Current management. *Neurologic Clinics, 21*(4), 883–895. https://doi.org/10.1016/S0733-8619(03)00016-1

Koleva, M., & De Jesus, O. (2023). Hydrocephalus. In StatPearls [Internet]. StatPearls Publishing. https://www.ncbi.nlm.nih.gov/books/NBK560875/

Kulkarni, A. V., Sgouros, S., Constantini, S., & IIHS Investigators. (2016). International Infant Hydrocephalus Study: Initial results of a prospective, multicenter comparison of endoscopic third ventriculostomy (ETV) and shunt for infant hydrocephalus. *Child's Nervous System, 32*(6), 1039–1048. https://doi.org/10.1007/s00381-016-3095-1

Lebel, C., & Deoni, S. (2018). The development of brain white matter microstructure. *NeuroImage, 182,* 207–218. https://doi.org/10.1016/j.neuroimage.2017.12.097

Ludwig, P. E., Reddy, V., & Varacallo, M. A. (2025). Neuroanatomy, central nervous system (CNS). In StatPearls [Internet]. StatPearls Publishing. https://www.ncbi.nlm.nih.gov/books/NBK442010/

Maller, V. V., & Gray, R. I. (2016). Noncommunicating hydrocephalus. *Seminars in Ultrasound, CT and MRI, 37*(2), 109–119. https://doi.org/10.1053/j.sult.2015.12.004

National Institute of Neurological Disorders and Stroke. (n.d.). Hydrocephalus. National Institutes of Health. Retrieved May 6, 2025, from https://www.ninds.nih.gov/health-information/disorders/hydrocephalus

Patel, S. K., Zamorano-Fernandez, J., Nagaraj, U., et al. (2020). Not all ventriculomegaly is created equal: Diagnostic overview of fetal, neonatal and pediatric ventriculomegaly. *Child's Nervous System, 36,* 1681–1696. https://doi.org/10.1007/s00381-019-04384-w

Peña Pino, I., Fellows, E., McGovern, R. A., Chen, C. C., & Sandoval-Garcia, C. (2024). Structural and functional connectivity in hydrocephalus: A scoping review. *Neurosurgical Review, 47*(1), 201. https://doi.org/10.1007/s10143-024-02430-z

Wright, Z., Larrew, T. W., & Eskandari, R. (2016). Pediatric hydrocephalus: Current state of diagnosis and treatment. *Pediatrics in Review, 37*(11), 478–490. https://doi.org/10.1542/pir.2015-0134

Yushkevich, P. A., Pashchinskiy, A., Oguz, I., Mohan, S., Schmitt, J. E., Stein, J. M., Zukić, D., Vicory, J., McCormick, M., Yushkevich, N., Schwartz, N., Gao, Y., & Gerig, G. (2019). User-guided segmentation of multi-modality medical imaging datasets with ITK-SNAP. *Neuroinformatics, 17*(1), 83–102. https://doi.org/10.1007/s12021-018-9385-x